

1 **Three-dimensional visualization of predatory gastropod feeding teeth with synchrotron scanning**

2

3 Gregory S. Herbert¹, Stephen A. Hill^{1,7}, Maria Jose Pio², Ryan Carney³, Amber Carlson¹, Elis Newham^{4,5},
4 Jen A. Bright^{1,6}

5

6 ¹ School of Geosciences, University of South Florida, Tampa, Florida 33620 USA

7 ² Consejo Nacional de Investigaciones Científicas y Técnicas, CONICET, Buenos Aires, C1425FQB
8 Argentina

9 ³ Department of Integrative Biology, University of South Florida, Tampa, Florida 33620 USA

10 ⁴ School of Engineering and Materials Sciences, Queen Mary University of London, London, UK

11 ⁵ Section Palaeontology, Institute of Geosciences, Rheinische Friedrich-Wilhelms-Universität Bonn,
12 Bonn, Germany

13 ⁶ Current Address: School of Natural Sciences, University of Hull, Hull, UK

14 ⁷ Current Address: Department of Earth and Planetary Sciences, University of Tennessee, Knoxville,
15 Tennessee 37996, USA

16

17 Correspondence: gherbert@usf.edu, j.bright@hull.ac.uk

18

19 **Keywords:** Gastropoda, Muricidae, radula, morphology, synchrotron

20

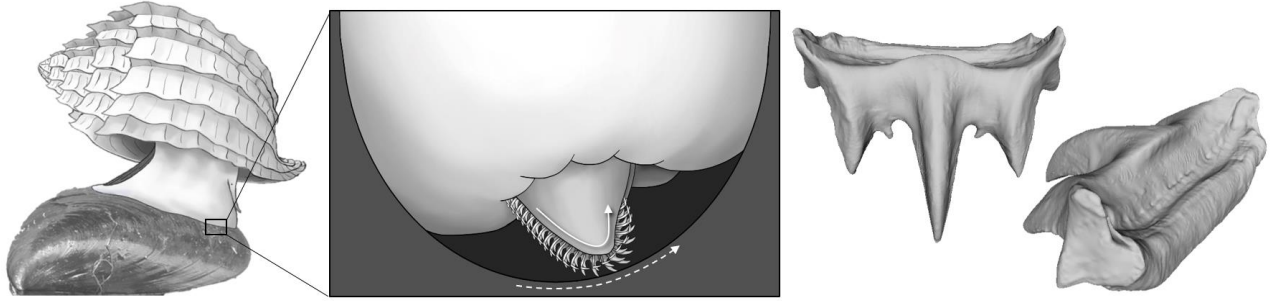
21 **Research Highlights:** Mineralized feeding teeth of four species of the gastropod family Muricidae are
22 imaged using synchrotron tomographic microscopy to explore features not viewed previously and
23 assemble 3D models to visualize tooth-tooth interactions as they would occur when drilling holes through
24 mineralized prey shells. We describe two new types of articulating joints, one of which increases contact
25 between teeth even as they rotate away from each other during drilling. Articulating joints have not been
26 described in Neogastropod radula previously but are consistent with earlier hypotheses that impact forces
27 on individual teeth during predatory drilling might be dispersed by tooth-tooth interactions.

28

29 This is the peer reviewed version of the following article: Herbert, G. S., Hill, S. A., Pio, M. J., Carney, R., Carlson, A.,
30 Newham, E., & Bright, J. A. (2023). Three-dimensional visualization of predatory gastropod feeding teeth with
31 synchrotron scanning. *Journal of Morphology*, 284, e21633, which has been published in final form at <https://doi.org/10.1002/jmor.21633>. This article may be used for non-commercial purposes in accordance with Wiley Terms and
32 Conditions for Use of Self-Archived Versions. This article may not be enhanced, enriched or otherwise transformed into a
33 derivative work, without express permission from Wiley or by statutory rights under applicable legislation. Copyright
34 notices must not be removed, obscured or modified. The article must be linked to Wiley's version of record on Wiley
Online Library and any embedding, framing or otherwise making available the article or pages thereof by third parties
from platforms, services and websites other than Wiley Online Library must be prohibited.

34

35 **Graphical abstract:**



36

37

38 A muricid snail feeding on a mussel prey by drilling a hole through its shell. Drilling involves chemical
39 softening agents secreted by an organ in the foot but also the radula, a ribbon of mineralized feeding teeth
40 in the proboscis that mechanically bores into the shell. The three-dimensional tooth shapes are described
41 for muricids for the first time using synchrotron tomographic microscopy, showing previously
42 undescribed saddle and tongue-and-groove joints between articulating teeth. These articulation surfaces,
43 which are mostly absent or underdeveloped in other neogastropods, support the hypothesis that muricid
44 tooth shape has evolved to minimize injury to the snail during drilling by distributing impact forces
45 between teeth.

46

47

48 **ABSTRACT**

49 Several families of neogastropod mollusks independently evolved the ability to drill through mineralized
50 prey skeletons using their own mineralized feeding teeth, sometimes with shell softening chemical agents
51 produced by an organ in the foot. Teeth with more durable tooth shapes should extend their use and
52 improve predator performance, but past studies have described only the cusped-side of teeth, mostly
53 overlooking morphologies related to functional interactions between them. Here, we describe the three-
54 dimensional morphology of the central drilling tooth (rachidian) from four species of the neogastropod
55 family Muricidae using synchrotron tomographic microscopy and assemble a 3D model of a multi-tooth
56 series in drilling position for two of them to investigate their dynamic form. We find two new types of
57 articulating surfaces, including a saddle joint at either end of the rachidian and a large tongue-and-groove
58 joint in the center. The latter has a shape that maximizes contact surface area between teeth as they rotate
59 away from each other during drilling. Articulating joints have not been described in Neogastropod radula
60 previously, but they are consistent with an earlier hypothesis that impact forces on individual teeth during
61 predatory drilling are dispersed by tooth-tooth interactions.

62

63 **1 INTRODUCTION**

64 Nearly all predatory families of gastropods arose in the late Cretaceous (Taylor et al., 1998), which was a
65 time of rapid evolutionary innovation and ecological restructuring now known as the Mesozoic marine
66 revolution (MMR) (Vermeij, 1977). One of the feeding innovations that evolved repeatedly during the
67 MMR was predatory drilling (Morton and Chan, 1997; Kabat, 1990; Ponder and Taylor, 1992), which
68 refers to the ability of some gastropods to excavate feeding holes through the mineralized armor of
69 shelled invertebrate prey. In the neogastropod family Muricidae, the most diverse clade of drillers,
70 drilling is thought to be the plesiomorphic mode of feeding (Vermeij and Carlson, 2000) and enabled by
71 alternating rounds of chemical dissolution by an accessory boring organ (ABO) and mechanical abrasion
72 by the radula, which consists of hundreds of rows of mineralized teeth attached to a long, flexible ribbon
73 (Carriker and Van Zandt, 1972; Carriker, 1981; Carriker and Gruber, 1999; Fig. 1). Each tooth row has a
74 multi-cusped rachidian tooth in the center flanked by a sickle-shaped lateral tooth on either side. During
75 the mechanical phase of drilling, the radular ribbon is pulled back and forth (Simone, 2011: 194) over the
76 tip of a tongue-like cartilage (the odontophore) like the teeth of a chain saw (Huxley, 1853), with each
77 pull causing contact of 5 to 15% of radula tooth rows with the prey shell surface (Hemingway, 1975;
78 Fujioka, 1985; Harding et al., 2008). Most of the tooth-substrate contact is with the rachidian tooth;
79 lateral teeth are pulled back and make only incidental contact with the surface (Carriker et al., 1974).
80 Simultaneously, the odontophore cartilage performs its own complicated motion, performing either a

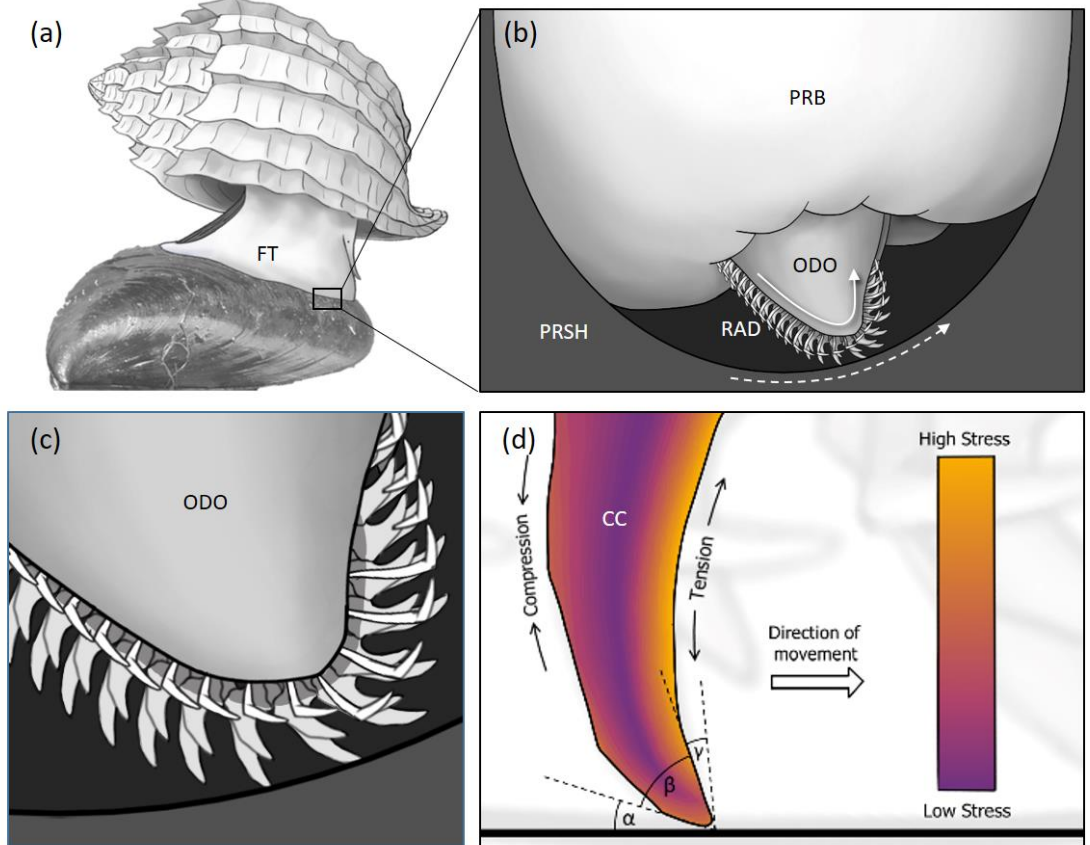
81 cleaning sweep across the prey shell surface or striking at it as a geologist would use a rock hammer
82 (Carriker and Schaadt, 1973; Carriker et al., 1974).

83
84 Tooth rows damaged from drilling (Fig. 2; Carriker et al., 1974) are continuously replaced in conveyer-
85 belt fashion, with upstream production of new teeth in the radular sac and downstream shedding of older
86 teeth into the esophagus. However, tooth damage from drilling can outpace the rate new teeth are moved
87 into striking position (Fujioka, 1985), leaving snails to reuse damaged teeth until nothing is left but a flat
88 base (Fig. 2d-f; see also Carriker et al., 1974). Selection should, therefore, favor (1) teeth with stronger
89 material properties (e.g., microstructural fibers, mineral reinforcement, degree of tanning) (Tyler and
90 Schiffbauer, 2012; Krings et al., 2022a), (2) faster tooth replacement (Fujioka, 1985), (3) evolution of
91 feeding modes that reduce drilling times (e.g., edge drilling, toxins, prying and wedging, scavenging,
92 parasitism) (Herbert, 2004, 2009; Dietl and Herbert, 2005; Paul et al., 2015); and/or (4) teeth with more
93 durable shapes that extend their use (e.g., self-sharpening wear, cusps with wider and stronger bases,
94 articulating bases, etc.) (Herbert et al., 2007, 2016).

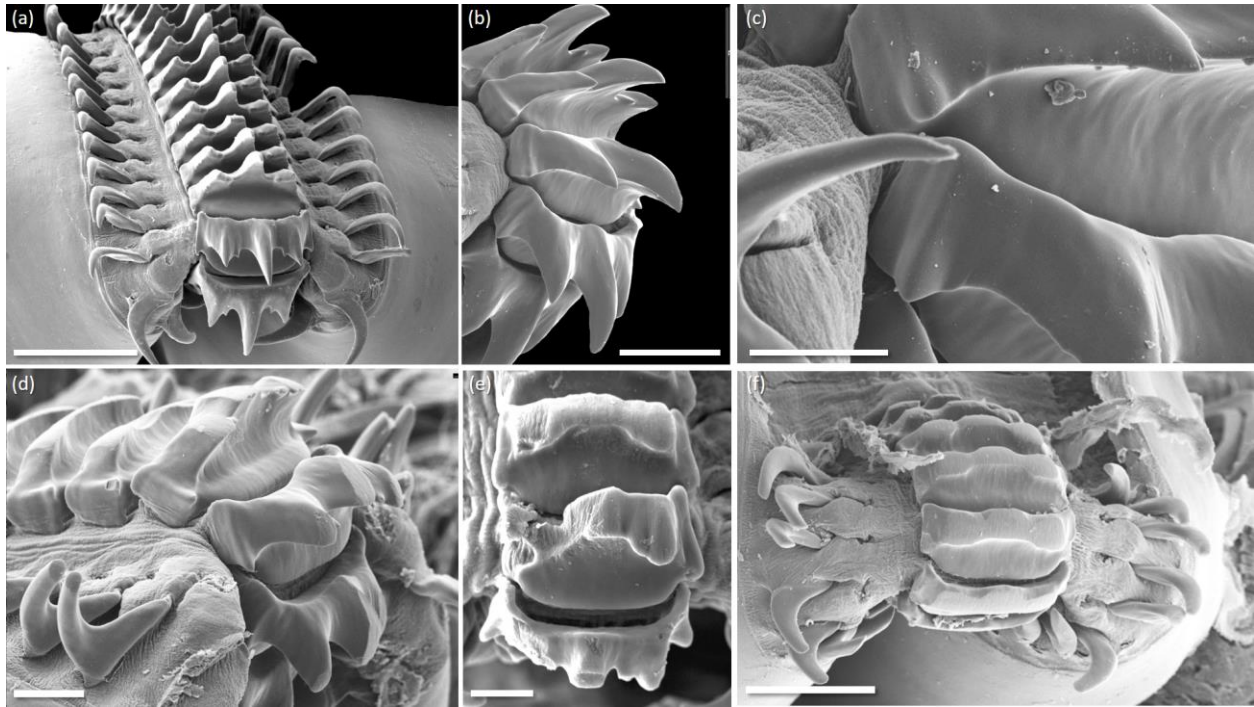
95
96 Complex articulating structures at the margins and bases of adjacent radular teeth are already known from
97 scanning electron micrographs (SEM) of muricid radulae (Pio et al., 2014; Herbert et al., 2015). Possible
98 functions of these structures include distributing impact forces between teeth to prevent early wear
99 (Carriker et al., 1974) and counteracting lateral bending or torsional forces along the radula by keeping
100 teeth aligned (Hickman, 1980, 1984). Interestingly, complex tooth-tooth articulation is absent or poorly
101 developed in neogastropods that use the radula for piercing, raking, or scooping soft flesh, reinforcing the
102 hypothesis that the complex articulations of muricid radulae are adaptations for drilling.

103
104 This study uses synchrotron tomographic microscopy (see Donoghue et al., 2006) to develop the first 3D
105 models of muricid radulae, a first step in testing whether ~70 million years of drilling has led to more
106 durable tooth shapes and better drillers. Synchrotron radiation produces extremely bright x-rays, allowing
107 much higher tomographic resolutions and better contrast than conventional medical- or micro-CT
108 scanners (Cunningham et al., 2014). Reconstructing tomographic x-ray data allows us to visualize
109 complete quantitative surfaces of muricid radulae from any orientation for the first time, including
110 articulation surfaces between teeth and between teeth and the supporting radular ribbon behind it. We also
111 show how 3D models of individual teeth can be assembled to better understand the dynamic form of the
112 radula during drilling, as opposed to relying on single-tooth morphology. From these reconstructions, we
113 report new features of muricid radulae, describe their variation in species representing several of the
114 muricid subfamilies, illustrate articulation surfaces and how interactions between teeth vary during

115 drilling, and formulate predictions about their putative functions in drilling that can be tested in the future
 116 with methods such as finite element analysis.
 117



118
 119 Fig. 1. Drawing showing the anatomical position of the feeding apparatus of the Muricidae during
 120 predatory drilling of a prey bivalve mollusk (a), excavation of shell inside an active borehole with a
 121 sweeping motion of the tooth-covered, odontophore-like tongue (dotted line) and simultaneous rotation of
 122 radular teeth over the tip of the odontophore (solid line) modeled after Carriker and Van Zandt (1972,
 123 figs. 12, 17) (b), closeup of individual central teeth (rachidia) of the radula striking the shell (c), and a
 124 schematic representation of how mechanical stresses on the rachidian tooth central cusp are likely to be
 125 accommodated as bending within striking cusps (d). CC = central cusp, FT = foot, ODO = odontophore,
 126 PRB = proboscis, PRSH = prey shell, RT = rachidian tooth, RAD = radula, α = clearance angle, β =
 127 wedge angle, γ = rake angle.
 128



129
 130 Fig. 2. Scanning electron micrographs (SEM) showing radular tooth-tooth contact and teeth before and
 131 after predatory shell drilling in the muricid *Trophon geversianus*. View of intact tooth rows, including the
 132 central rachidian tooth and sickle-shaped outer lateral teeth, as the radula rotates over the odontophore tip
 133 (a). Lateral view of unworn articulating rachidian teeth (b). Closeup of unworn marginal cusps of a
 134 rachidian tooth (c). Central and lateral cusps maintain sharp edges after wear, extending tooth lifespan (d).
 135 Heavy wear and structural failure of rachidian tooth central and lateral cusps (e). Complete wear of
 136 rachidian tooth cusps and latero-marginal ridge (f). Rachidian tooth terminology explained in Fig 3. Scale
 137 bars = 200 μm (a), 100 μm (b), 20 μm (c), 50 μm (d), 20 μm (e), 100 μm (f).

138
 139

140 2 MATERIALS AND METHODS

141 2.1 Specimen preparation

142 Species selected for synchrotron imaging included one individual each of *Muricanthus ambiguus* (Reeve,
 143 1845) (subfamily Muricinae) (78 mm shell length), *Thaisella kiosquiformis* (Duclos, 1832) (34 m shell
 144 length), and *Acanthais triangularis* (Blainville, 1832) (21 mm shell length) (both subfamily Rapaninae)
 145 from near Venado Island, Panama, and *Trophon geversianus* (Pallas, 1774) (subfamily Trophoninae) (35
 146 mm shell length) from Puerto Madryn, Argentina. Radulae were isolated from full-sized, adult specimens
 147 preserved in 70% ethanol by dissecting the proboscis and dissolving the buccal mass tissues in
 148 concentrated sodium hypochlorite. Radulae were collected with forceps, washed in distilled water,
 149 snipped with forceps into three or four shorter segments, and one or two individual segments fastened

150 cusps-side-up while still wet in open position (lateral teeth pulled away from the rachidian as with a
151 typical SEM mount) on the end of a 2 mm wide carbon fibre rod with polyvinyl acetate (washable
152 Elmer's PVA glue) and allowed to air dry.

153
154 To visualize tooth wear and the radula in its functional feeding position (Fig. 2), odontophores were
155 dissected from the proboscises of several individuals of *T. geversianus*, dehydrated in a graded ethanol
156 series, critical point dried, and attached to SEM tabs with double-sided conductive tape for SEM imaging.
157 The smoothness of the radular membrane and the positions of interlocking teeth (e.g., Fig. 2a) show that
158 deformation of the radulae during drying was minimal.

159 160 **2.2 Scanning procedures and 3D-modeling**

161 Specimens were scanned using single propagation distance phase contrast tomography at the European
162 Synchrotron Radiation Facility (ESRF) in Grenoble, France using the ID19 microtomography beamline.
163 Every specimen used the following scan parameters: 2999 angular projections collected for a 360°
164 rotation; 0.1 ms exposure time; 360 nm³ voxel size; 20 mm sample-to-detector distance; x-ray energy of
165 26.5 keV. Preparation of critical point dried specimens for SEM was the same as for synchrotron
166 preparation except that radulae were coated with Au-Pd and mounted on stubs with double-sided
167 conductive tape for imaging with a Philips XL 30 scanning electron microscope at the Museo Argentino
168 de Ciencias Naturales.

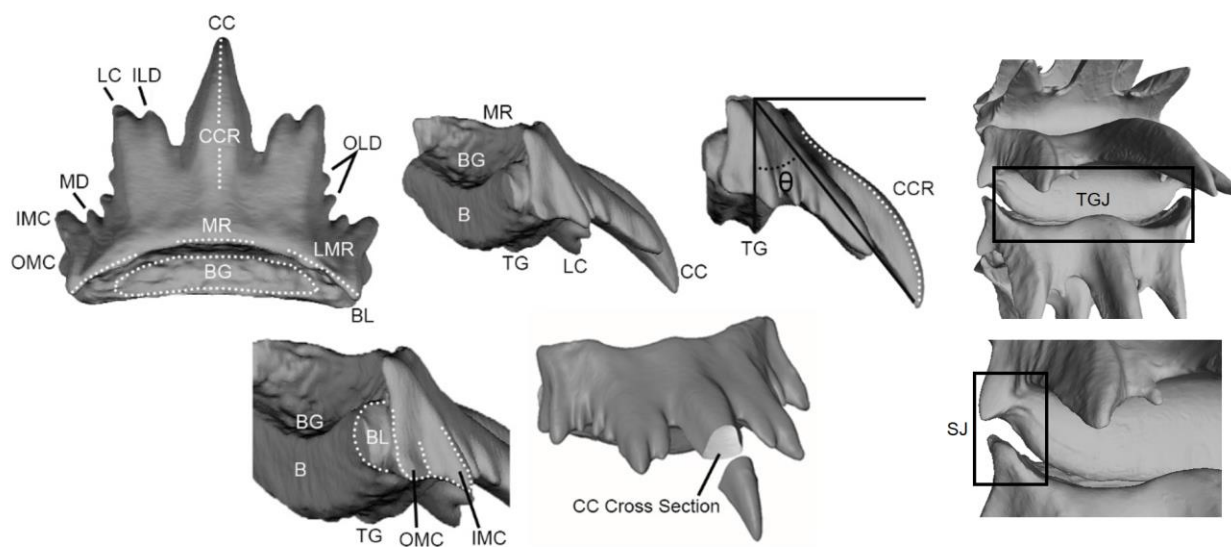
169
170 Sixteen-bit Synchrotron *.tif stacks were reconstructed using "Paganin" single-distance phase retrieval
171 algorithms (developed in-house at ID19), imported into *Avizo Lite 9.4* (Thermo Fisher Scientific), and
172 visually explored for mature rachidian teeth that showed no evidence of *in vivo* wear or post-mortem
173 breaking during sample preparation. The scan volume was then cropped to these sections to facilitate data
174 management. Segmentation of one tooth per species was performed semi-automatically: the "Magic
175 Wand" tool was used initially to select the tooth volume based on greyscale intensity and then to
176 manually remove any traces of the supporting radular membrane, mount, or mounting glue that remained
177 attached to the teeth. Once segmented, each tooth was exported as an *.stl and brought into *Geomagic*
178 *Wrap 2017* (3D Systems) for smoothing and cleaning of artefacts. In one specimen (*Acanthais*), damage
179 to the tooth was only apparent after segmentation.

180
181 Although not all muricid radulae are symmetrical (e.g., muricid subfamily Typhinae), most are, and we
182 assumed bilateral symmetry and used palaeontological protocols (Lautenschlager, 2016) to reposition and
183 retro-deform damaged cusps of the *Acanthais* tooth in *Geomagic* and *Avizo*. Damage to the *Acanthais*

184 specimen was addressed by creating an individual segmentation of the detached marginal cusp, which
 185 was then aligned to the body of the main tooth in *Avizo* and the surfaces combined in *Geomagic* using the
 186 “merge” function. The merged file was then reimported into *Avizo* where minor cracks were filled and the
 187 model was smoothed. The central cusp was repaired by selecting a “donor cusp” from an undeformed
 188 tooth from the same radula and segmenting it. The deformed central cusp from the original specimen was
 189 removed and the donor cusp aligned and merged into its place using the same methods previously applied
 190 to the marginal cusp. Segmenting artefacts in the form of ridges on the central cusp were removed by
 191 smoothing.

192
 193 Rachidian base widths were measured at the widest point and are reported for individual teeth selected for
 194 segmentation. Measurements of the cusp angle from the rachidian base were taken digitally using Adobe
 195 Photoshop (version 22.4) in lateral profile. A line parallel to the radular ribbon was drawn from the apex
 196 of the tongue and projected to the equivalent position on the trailing side. An angle was then taken from
 197 this line to the tip of the cusps on the feeding side (Fig. 3). Cross sections of the central cusp were taken
 198 in MeshLab v.2020.02 (Cignoni et al., 2008). A plane was defined at halfway along the trailing length of
 199 the central cusp and material distal to this plane was removed. The sectional view was oriented in the
 200 plane of the screen and traced in Photoshop. Anatomical terminology for rachidian features described
 201 previously follows Kool (1993) and Pio et al. (2014), with some new features described herein for the
 202 first time.

203



204

205 Fig. 3. Rachidian tooth terminology. B = Base; BG = basal groove; BL = basal lobe; CC = central cusp;
 206 CCR = central cusp ridge; ILD = inner lateral denticle; IMC = interior marginal cusp; LC = lateral cusp;

207 LMR = latero-marginal ridge; MD = marginal denticle; MR = medial ridge; OLD = outer lateral denticle;
208 OMC = outer marginal cusp; SJ = saddle joint; TG = tongue; TGJ = tongue and groove joint; θ = cusp
209 projection angle.

210

211 **2.3 Analysis of tooth-tooth contact during rotation over the odontophore**

212 To visualize how tooth articulation surfaces interact during rotation of the radula over the odontophore,
213 the 3D models of a segmented tooth from *T. geversianus* and *T. kiosquiformis* were duplicated and used
214 to reconstruct two articulated radular series of five teeth, from which cross sections and deviation maps
215 were generated for teeth away from and at the bending plane of the odontophore. The *Remesh* function of
216 *Geomagic Wrap 2017* was used to decimate the *T. kiosquiformis* model to 500K polygons (originally
217 4.4M; *T. geversianus* model was 493K). For *T. geversianus*, and using *Maya 2023* (Autodesk), a
218 polygonal cube was created, flattened, and positioned to represent the radular ribbon attachment and
219 thickness, based on a reference image from the scans (SI 1). This ribbon object delineated the borders of
220 the ventral surface of the radula that articulates with the odontophore. Within this ventral surface, a
221 rectangular strip of polygons was selected in *Geomagic Wrap 2017*. A cylinder was algorithmically fit to
222 these polygons using the *Best Fit* function and imported into *Maya* using custom MEL scripts to define
223 the center of rotation and rotational axis Z of an XYZ locator object (Carney in revision). In *Maya*, the Y
224 axis of this object was aligned to the ribbon object plane, yielding an X axis that bisected the ventral
225 articular surface. The tooth was then parented under the XYZ locator object, which in turn was translated
226 and oriented to the world origin (0,0,0). Both the cylinder-based axes and inertial axes (via custom
227 MATLAB script; Ibid.) revealed $\sim 2^\circ$ of bilateral asymmetry in the tooth, which was compensated for in
228 order to align the central cusp axis to the world axis. Inertial axes were also created for the *T.*
229 *kiosquiformis* tooth and used to translate and orient this model to the world origin, as well as for
230 subsequent rotations of the other teeth in the radular series (0, 22.5, 45, and 45 degrees between each pair
231 from left to right). $\sim 1^\circ$ of bilateral asymmetry was apparent in this tooth. However, a compensatory
232 rotation resulted in poorer alignment between teeth in the radular series and so was not used for the final
233 reconstruction. For *T. geversianus*, SEM images (e.g., Fig. 2b) were projected onto the *Image Plane* of
234 virtual cameras, the middle tooth of which was aligned to the 3D model and used as a reference for
235 manually positioning four instanced duplicates of the tooth into an articulated series (two in front, two in
236 back). Contiguity of the ribbon objects was maintained for the *T. geversianus* series, and interpenetration
237 of the tooth models was avoided. A sagittal section was created to visualize the articulations along the
238 axis of the central cusp for both species. Deviation maps between adjacent teeth were generated by
239 importing the articulated series from *Maya* into *Geomagic Wrap 2017*, post-processing the model meshes
240 (*Mesh Doctor*), flipping the normals of the anterior tooth (*Flip Normals*), and then selecting the posterior

241 tooth for analysis (*Deviation*; with a critical angle of 45° and a maximum deviation of 20 and 10 µm for
242 *T. geversianus* and *T. kiosquiformis*, respectively).

243

244 **3 RESULTS**

245 **3.1 3D Model Descriptions**

246 *Trophon geversianus* (Pallas, 1774) (Trophoninae) (Fig. 4a). Rachidian tooth width 203 µm. Central cusp
247 long, narrow, gently curved along sagittal axis, with 60° degree angle of projection from rachidian base.
248 Central cusp cross-section triangular with rounded angles (Fig. 5a), resulting in a narrow, rounded central
249 cusp ridge. Lateral cusps short, roughly half the length of central cusp, triangular shape with wide base,
250 bent downward (ventrally) mid-way along sagittal axis, and with 41° angle of projection from rachidian
251 base. Inner edge of lateral cusps smooth, outer edge with 3 low serrations. One inner lateral denticle
252 between central and each lateral cusp. Inner lateral denticles short, thin, sharing a common base with
253 lateral cusp, oriented at 45° angle towards central cusp. Marginal area narrow with one low marginal
254 denticle. Two marginal cusps at each end of rachidian base. Inner marginal cusp short, narrow, and
255 sharply pointed, with distal end gently curved laterally and forward (dorsally). Outer marginal cusp
256 weakly developed as a faint ridge mid-way between inner marginal cusp and short, semi-circle-shaped
257 basal lobe. Latero-marginal ridge narrow, restricted to marginal cusp zone. Rachidian base thick with
258 broad, straight basal groove overlapped by prominent M-shaped medial ridge; large, rounded tongue.
259 Medial ridge broad, rounded.

260

261 *Muricanthus ambiguus* (Reeve, 1845) (Muricinae) (Fig. 4b). Rachidian tooth width 229 µm. Central cusp
262 long, narrow, gently curved along sagittal axis, with 43° degree angle of projection from rachidian base.
263 Central cusp parabolic in cross section (Fig. 5b), resulting in prominent, rounded central cusp ridge.
264 Lateral cusps long, narrow, more than half the length of central cusp, gently curved along axis, with 42°
265 angle of projection from rachidian base. Inner edge of lateral cusps with single, low serration at
266 midlength; outer edge smooth. One inner lateral denticle between central and each lateral cusp. Inner
267 lateral denticles thin, free from lateral cusp, slightly recurved laterally. Marginal area narrow, smooth,
268 arched. Marginal cusps absent. End of rachidian base rounded. Basal lobe small, semi-circular. Latero-
269 marginal ridge high, rounded, and broad, extending from marginal area to lateral cusp zone. Rachidian
270 base thin, U-shaped with broad, shallow, U-shaped basal groove and tongue. Medial ridge narrow, low.

271

272 *Acanthais triangularis* (Blainville, 1832) (Rapaninae) (Fig. 4c). Rachidian tooth width 92 µm. Central
273 cusp is long, narrow, gently curved along sagittal axis, with 36° degree angle of projection from rachidian
274 base. Central cusp cross-section is an oblate circle (Fig. 5c), resulting in broad, rounded central cusp

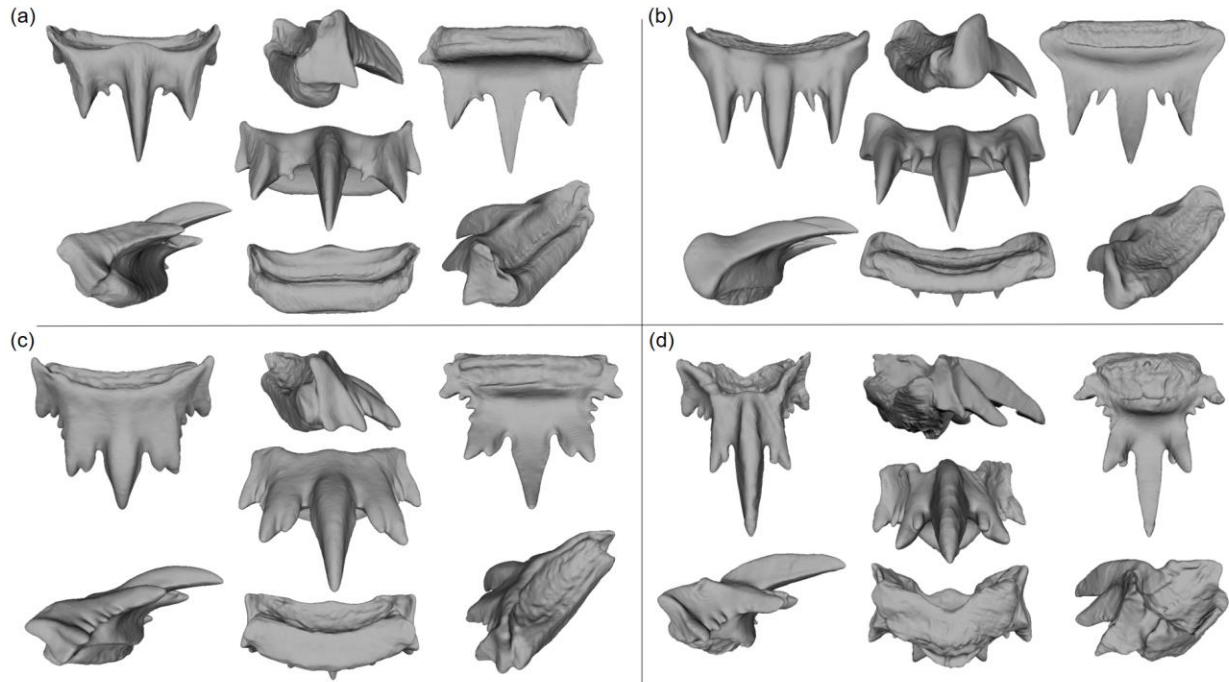
275 ridge. Lateral cusps long, more than half the length of central cusp, triangular shape with wide base, slight
276 lateral deflection, and 35° angle of projection from rachidian base. Inner edge of lateral cusps smooth,
277 outer edge with 2 large, denticle-like serrations. One inner lateral denticle between central and each
278 lateral cusp. Inner lateral denticles long, bullet-shaped, sharing a common base with lateral cusp, and
279 slightly laterally deflected. Marginal area narrow with one large marginal denticle. Two marginal cusps at
280 each end of rachidian base. Inner marginal cusp long, bullet shaped, with distal end gently curved
281 laterally. Outer marginal cusp smaller, weakly developed, in front of prominent, pointed basal lobe.
282 Latero-marginal ridge flat-topped, broad, extending from marginal area to lateral cusp zone. Rachidian
283 base thick with deep, U-shaped basal groove and narrow, weakly developed medial ridge; shallow,
284 rounded tongue.

285

286 *Thaisella kiosquiformis* (Duclos, 1832) (Rapaninae) (Fig. 4d). Rachidian tooth width 71 µm. Central cusp
287 is long, narrow, with gentle curve along sagittal axis and 48° degree angle of projection from rachidian
288 base. Central cusp cross-section resembles a trapezoid (Fig. 5d), resulting in sharp, high central cusp
289 ridge. Lateral cusps half the length of central cusp, with triangular shape, prominent ridge, wide base,
290 slight lateral deflection, and 34° angle of projection from rachidian base. Inner edge of lateral cusps
291 smooth, outer edge lacking serrations. One inner lateral denticle between central and each lateral cusp.
292 Inner lateral denticles short, narrow, sharing a common base with lateral cusp. Marginal area wide with 2
293 large marginal denticles. Two marginal cusps at each end of rachidian base. Inner marginal cusp long,
294 narrow, with distal end gently curved laterally. Outer marginal cusp small, weakly developed, in front of
295 heavy, knob-like basal lobe. Latero-marginal ridge low, broad, extending from marginal area to lateral
296 cusp zone. Rachidian base thick with a broad medial ridge and deep, bowl-shaped basal groove; narrow,
297 rounded tongue.

298

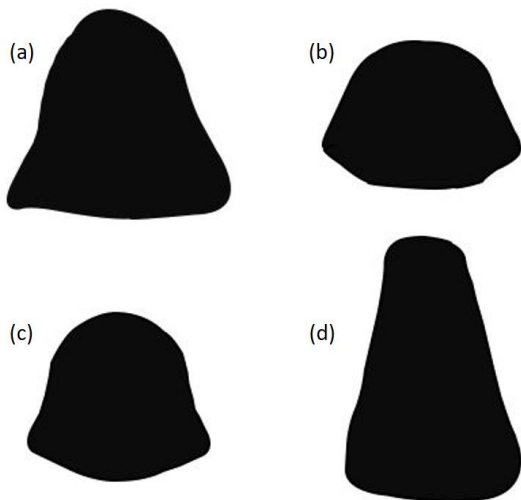
299



300
 301 Fig. 4. 3D renderings of rachidian teeth of *Trophon geversianus* (a), *Muricanthus ambiguus* (b),
 302 *Acanthais triangularis* (c), *Thaisella kiosquiformis* (d). See Results text for tooth widths.

303
 304 **3.2 Central Cusp Cross-Sectional and Medial Ridge Shapes**

305 The central cusp shafts of *Trophon*, *Muricanthus*, and *Acanthais* are bell-shaped and more or less oblate
 306 in cross-section, while the cross section of the central cusp of *Thaisella* is more trapezoidal (Fig. 5). The
 307 medial ridge ranges from a narrow and prominent ridge in *Thaisella* and *Trophon* to only a weakly
 308 developed hump in *Muricanthus* and *Acanthais* (Fig. 5).



309

310 Fig. 5. Central cusp cross sections for *Trophon geversianus* (a), *Muricanthus ambiguus* (b), *Acanthais*
311 *triangularis* (c), and *Thaisella kiosquiformis* (d).

312

313 **3.3 Observations on Material Composition**

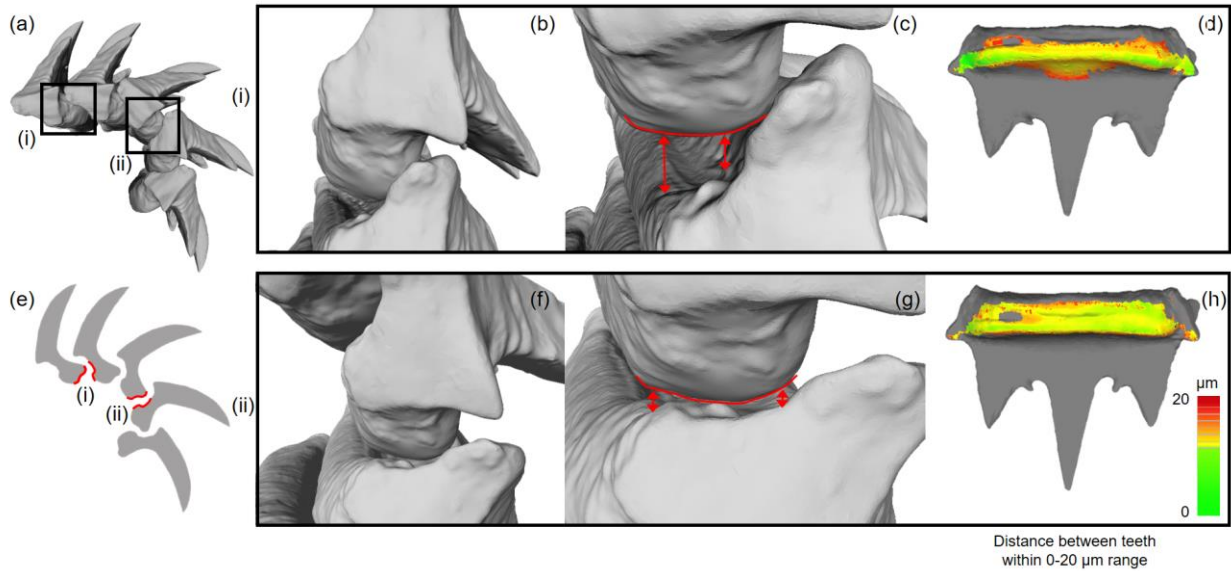
314 No differences in radiodensity, which might indicate variation in internal structure, chemical composition,
315 or mineralisation, were detected within teeth or between the teeth, radular ribbon, and PVA adhesive used
316 to mount the specimens (Fig. SI).

317

318 **3.4 Articulation Surfaces in 3D**

319 SEMs and our 3D reconstructions of the radula of *T. geversianus* show that the tongue-and-groove joint
320 tightens posteriorly as the teeth rotate over the tip of the bending plane of the odontophore, even as the
321 angle between central cusps of adjacent teeth increases (Figs. 2a-f, 6). Conversely, the saddle joint at the
322 marginal cusps becomes more open for *T. geversianus*. For *T. kiosquiformis*, the tongue-and-groove joint
323 also tightens posteriorly for teeth near the bending plane of the odontophore, but the extent of tightening
324 across the tongue is much less due to the much greater depth of the basal groove in *T. kiosquiformis* (Fig.
325 7). Distances between articulation surfaces of the saddle joints in *T. kiosquiformis* show little change in
326 teeth further from and closer to the bending plane of the odontophore.

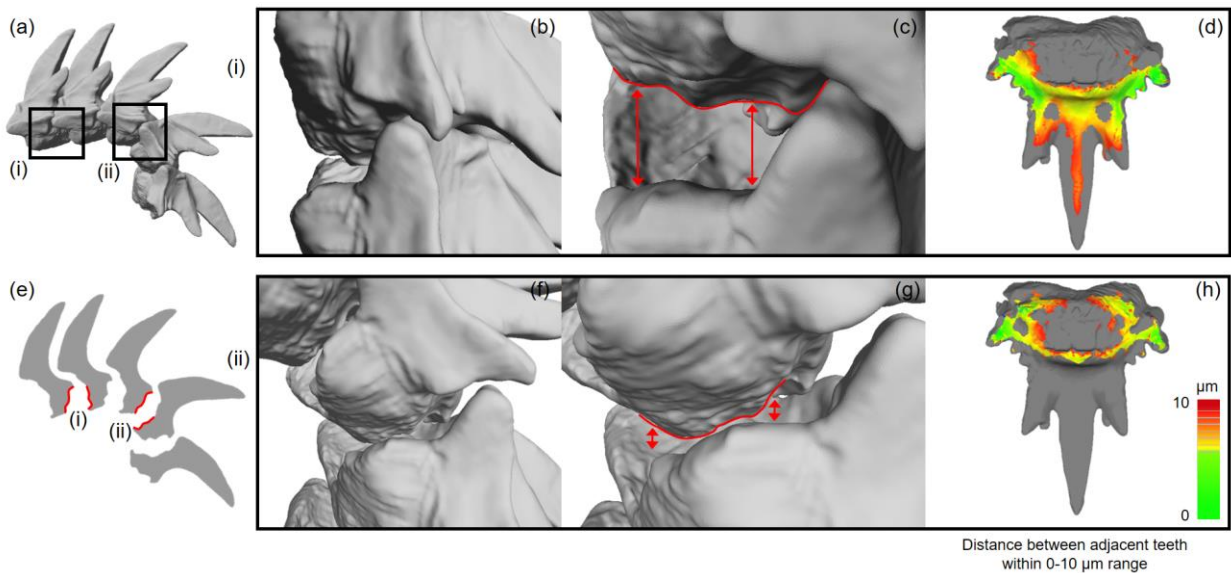
327



328

329 Fig. 6. Articulated series of five duplicated tooth models of *Trophon geversianus* (a), showing tooth-tooth
 330 articulation (b, c, f, g). Sagittal section through the central cusp of the five articulated teeth, with the
 331 sigmoidal outlines of the tongue-and-groove articulation surface highlighted in red for teeth further away
 332 (i) and closer to the bending plane of the odontophore tip (ii) (e). Deviation maps illustrating distances
 333 between articulating surfaces of adjacent teeth in minimum (i) and maximum (ii) relative rotation; heat
 334 map with a linear scale of $\pm 20 \mu\text{m}$ (d, h). Note the expansion of the tongue-and-groove articular surface
 335 and slight reduction of the saddle joint articular surfaces in (f) compared to (d).

336



337

338 Fig. 7. Articulated series of five duplicated tooth models of *Thaisella kiosquiformis* (a), showing tooth-

339 tooth articulation (b, c, f, g). Sagittal section through the central cusp of the five articulated teeth, with the
340 sigmoidal outlines of the tongue-and-groove articulation surface highlighted in red for teeth further away
341 (i) and closer to the bending plane of the odontophore tip (ii) (e). Deviation maps illustrating distances
342 between articulating surfaces of adjacent teeth in minimum (i) and maximum (ii) relative rotation; heat
343 map with a linear scale of $\pm 20 \mu\text{m}$ (d, h). Note the posterior expansion of the tongue-and-groove
344 articular surface in (f) compared to (d), as in *T. geversianus*, except for a large central region of the
345 articulation surface.

346

347 **4 DISCUSSION**

348 **4.1 Major results**

349 Our synchrotron scans reveal the complete 3D morphology of the muricid rachidian for the first time,
350 including two previously undescribed types of articulation surfaces: (1) a tongue-and-groove system that
351 articulates adjacent tooth bases as a hinge joint, and (2) two saddle joints, one at each end of the rachidian
352 tooth formed by an arched shoulder (latero-marginal ridge) on the posterior tooth that fits within a notch
353 in the adjacent, anterior tooth. Our study also reveals substantial variation between species in the shapes
354 of these articulation surfaces and how they are formed (Fig.4).

355

356 The tongues of these tongue-and-groove joints vary most obviously in length but also degree of curvature,
357 the presence of ridges, and width of the attachment zone between the rachidian tooth and the backing
358 radular membrane. The corresponding groove varies from a rectangular depression that is open on one side
359 to a deep bowl-shaped depression. Variation in the saddle joint notch is determined primarily by which
360 features that create the notch. It is formed by the angle between two marginal cusps in some species,
361 while in others it forms between the lateral cusp and basal lobe, the marginal cusp and basal lobe, or the
362 outer marginal cusp and the basal lobe (Fig. 4; also Pio et al., 2014: figs. 1,3). There is also variation in
363 the position of the latero-marginal ridge (part of the adjacent tooth that fits within the saddle joint)
364 between species, which can form above each marginal cusp or each lateral cusp or span both (Fig. 4;
365 Herbert et al., 2007, 2015; Pio et al., 2014).

366

367 Although Carriker et al. (1974) did not describe specific articulation types, they hypothesized that “basal
368 support” in the muricid radula might be an adaptation for dispersing forces from violent impacts during
369 predatory shell drilling across multiple rachidian teeth, thereby preventing stress buildup within any
370 individual tooth. Experimental evidence for force dispersion by tooth-tooth contact has since been
371 demonstrated in other mollusks, including chitons and paludomid gastropods (Krings et al., 2021a;
372 2021b; 2022b). Our 3D reconstructions of 5-tooth rachidian series for *T. geversianus* and *T. kiosquiformis*

373 reveal that the articulation surfaces of the tongue-and-groove joint (Fig. 6e, 7e) become increasingly
374 parallel (i.e., improved fit) as teeth approach the striking tip of the odontophore. This may represent a
375 unique type of joint that has not yet been described. We hypothesize that if improved fit of the tongue-
376 and-groove surfaces of teeth at the striking tip of the odontophore exists *in vivo*, it would allow for tooth-
377 tooth contact to increase during drilling, along with increased potential for force dispersion between the
378 striking tooth and adjacent teeth. Thus, Carriker et al.'s (1974) hypothesis that tooth-tooth contact is
379 capable of dispersing impact forces during drilling is supported by our observations, but our study goes
380 further in showing how tooth fit and potential for force dispersion improve at the striking tip of the
381 odontophore. Future should explore how tooth-tooth fit over the odontophore varies across the Muricidae
382 and whether there is evidence for adaptive improvement, i.e., directional trends from more basal to more
383 recently evolved lineages.

384
385 Well-developed articulating bases are common but not ubiquitous across the Muricidae. The muricine *M.*
386 *ambiguus*, for example, has a relatively shallow tongue-and-groove hinge joint (Fig. 4b), and the anterior
387 end of the saddle hinge is formed by a shallow depression between the lateral cusp and base endpoint. In
388 contrast, the rapanine *T. kiosquiformis* has a deep tongue-and groove hinge and a saddle hinge developed
389 as a sharp notch between two marginal cusps (Fig. 4d). In general, simpler and more weakly-developed
390 articulating bases are found in the subfamilies Muricinae and Haustrinae; variable complexity and
391 development are found in the Rapaninae, Ergalataxinae, Muricopsinae, and Trophoninae; and complex
392 and strongly developed articulating bases are found in the Ocenebrinae (Herbert et al., 2007, 2015; Pio et
393 al., 2014). Since the Muricinae predates all other subfamilies in the fossil record by at least 20 million
394 years (Vermeij and Carlson, 2000; Merle, 2012), we propose that more complex tooth articulation was
395 absent in earliest muricids and evolved later as drilling increased in frequency as a mode of attack, as prey
396 shells thickened and drilling times increased, and/or as interactions between drillers and their own
397 predators intensified selection for more efficient drilling. Conversely, relaxation in selection for traits that
398 reduce stress and strain on teeth is expected in lineages where the use of drilling has given way to faster,
399 non-drilling feeding modes, such as use of toxins, shell chipping, and parasitism (Herbert, 2004; Dietl and
400 Herbert, 2005; Herbert et al., 2007, 2009, 2016, Pio et al., 2014; Paul et al., 2015). This hypothesis would
401 be most productively explored in subfamilies with the greatest diversity of articulation surfaces, well-
402 resolve phylogenies, and abundant feeding and dietary observations (e.g., Rapaninae).

403
404 Testing these hypotheses rigorously would require advances over previous work, which have tended to
405 focus on how radular teeth deform and distribute stresses and strain in isolation during feeding (Van der
406 Wal et al., 2000; Krings et al., 2020; Lee et al., 2023). While studying tooth performance in isolation can

407 give valuable insight into the structural performance of tooth morphology, interactions between adjacent
408 tooth bases must be factored in in studies of the muricid radula. Krings et al. (2021c) modelled a section
409 of a gastropod radula comprising multiple teeth embedded within the radula ribbon. This approach
410 permits some understanding of how different teeth respond to the same loading scenario. However, the
411 close tooth arrangement and highly dynamic motion of the radula as it passes over the odontophore tip in
412 muricids may require use of more computationally-complex, non-linear, large-displacement models with
413 well-defined, non-penetrating contact surfaces to fully resolve between-tooth strains (see Marcé-Nogué,
414 2022 for an in-depth discussion of these issues).

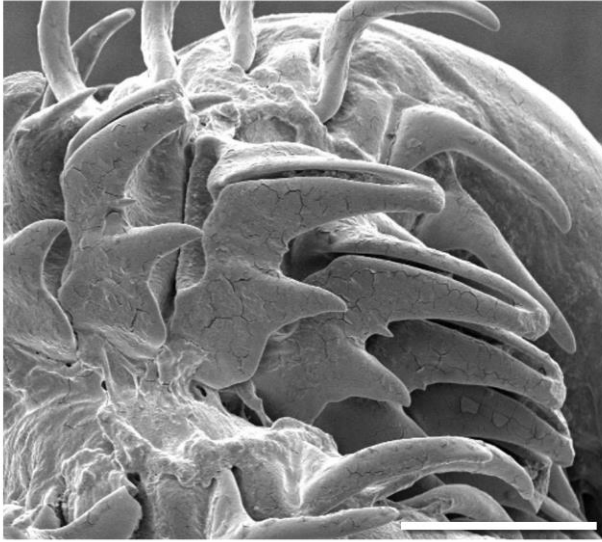
415

416 **4.2 Alternative explanations for saddle and tongue-and-groove joints**

417 An alternative explanation for tooth-tooth articulation features of gastropod radulae is that they counteract
418 bending and torsional forces along the radula during feeding by holding teeth in place (Hickman, 1980,
419 1984). This explanation could apply to saddle joints in some muricid species because of the way marginal
420 cusps wrap laterally around the adjacent tooth (e.g., *T. kiosquiformis*: Fig. 7f,g). This is supported by (1)
421 the fact that the saddle joints of *T. geversianus* are maximally open (least contact) when teeth are at the
422 striking tip of the odontophore, unlike its tongue-and-groove joint; and (2) observations of wear of the
423 latero-marginal ridge on teeth in several specimens of *T. geversianus* (Fig. 2d-f). The latter type of wear
424 can only be explained by tooth-tooth interactions since the latero-marginal ridge does not face the prey
425 shell surface.

426

427 An unexpected finding of our research was the large, circular area of no contact (a large open space) in
428 the center of the tongue-and-groove joint articulation surface of *T. kiosquiformis*, even when teeth are
429 rotated into feeding position and the tongue and groove fit is tightest (Fig. 7h). This open space is created
430 by a deep, basin-like groove and short tongue in *T. kiosquiformis*. The function of this deep basin is
431 unknown, but another rapanine, *Plicopurpura patula*, has a similar deep, basin-like groove that opens into
432 an open slit down the center of a long, hypodermic-needle-like central cusp (Fig. 8; also Kool, 1993: fig.
433 17e). Since hypodermic-needle-like teeth are associated with toxin delivery in other predatory gastropods
434 (Puillandre et al., 2017), basin-like depressions that open into the needle plausibly store toxins. Basin-like
435 grooves with poor tongue-and-groove surface articulation in other species could serve a similar function.
436 This hypothesis is speculative but mentioned as there are alternatives to purely biomechanical
437 explanations for tooth shape in the Muricidae.



438

439 Fig. 8. Radula of the rapanine muricid *Plicopurpura patula* showing deep, basin-like groove of the
440 rachidian base that connects to an open slit down the center of the central cusp. Scale bar = 100 μm .

441

442 **4.3 Distribution of articulating rachidian bases in the Neogastropoda**

443 Rachidian bases with articulating tongue-and-groove or saddle joints are either completely absent or
444 poorly developed in almost all other Neogastropoda outside of the Muricidae, including Buccinoidea
445 (Fedosov and Kantor, 2012; Harasewych, 2018), Olivoidea (Kantor and Bouchet, 2007; Kantor et al.,
446 2017), Conoidea (Kantor et al., 2018), Mitroidea (Fedosov et al., 2015, 2017) and Turbinelloidea (Kantor
447 et al., 2001). Most of these neogastropods use the radula for piercing, raking, and scooping soft prey
448 tissues rather than drilling through hard shell (Taylor, 1998). Exceptions include a small number of
449 species of Volutoidea (e.g., *Cysticus* sp.: Fedosov et al., 2019: fig. 4C,D) and Turbinelloidea
450 (*Ceratoxancus* spp: Kantor and Bouchet, 1997; *Cyomesus chaunax* Harasewych, 1987: fig. 20) that have
451 tooth-tooth contact, shallow- to moderately-deep tongue-and-groove articulation, and a present but
452 weakly-developed saddle joint (i.e., latero-marginal ridge bounded by one cusp). Kantor and Bouchet
453 (1997:119-20) speculated that at least one of these, *Ceratoxancus basileus*, drills shelled prey based on
454 SEMs of the radula showing rachidia worn flat to the base (Kantor and Bouchet, 1997: fig. 3B). Other
455 species of *Ceratoxancus* have been found to use a labral spine on the shell's aperture to wedge open large
456 bivalve prey (Kantor and Bouchet, 1997), a mode of attack also used by some muricids in combination
457 with drilling (Vermeij, 2001). Predation behaviors of *Cyomesus* and *Cysticus* are unknown, but their
458 rachidian morphology suggests they might also drill or chip shelled prey using the radula (Y. Kantor,
459 personal communication to GSH June 8, 2020). Given current knowledge of family-level phylogenetic
460 relationships among neogastropods (e.g., Fedosov et al., 2015), these sporadic occurrences of articulating
461 tooth bases outside the Muricidae probably represent independent origins.

462

463 **4.4 Biomechanics of the rachidian cusps**

464 **4.4.1 Cusp shape.** Our 3D scans illustrate morphological variation of rachidian cusps, ridges, and
465 denticles across the family. Muricid rachidia usually have three major cusps, including a long central cusp
466 flanked on each side by one lateral cusp (Herbert et al., 2007). Cusps come to a sharp point distally,
467 which helps generate fracture-inducing stresses in the prey shell. The cusp shaft functions as a
468 cantilevered beam that is loaded in bending when it contacts the prey shell. Stresses developed in a beam
469 under bending are dependent on both the cross-sectional shape of the beam (the second moment of area)
470 and the bending moments it experiences, which are themselves dependent on the length and curvature of
471 the beam, and the magnitude and direction of the loading force. Length and curvature of the cusps vary
472 widely between species and within species during ontogeny (Herbert et al., 2007, 2015; Pio et al., 2014).

473

474 Cusp cross-sectional shapes vary between species in the Muricidae, potentially affecting performance.
475 Although a trapezoidal cross section results in a blunter cusp tip and, thus, potentially lower fracture-
476 inducing stresses on the prey shell, Euler-Bernoulli beam theory predicts that under bending loads, such a
477 cross-section will be comparatively stronger in bending in the antero-posterior direction. As this is the
478 dominant loading direction during feeding, we predict that the trapezoidal cross-sectional cusp shape of *T.*
479 *kiosquiformis* should better resist bending stresses in the shaft relative to bell-shaped cross-sectional
480 shapes.

481

482 Curvature of the cusp along its main axis is also important, because forces from drilling produce higher
483 moment arms (and therefore stresses) in a straight cusp than in a curved one. Using 2D finite element
484 analysis, Van der Wal et al. (2000) showed that a curved cusp shifts stresses away from the tooth tip and
485 towards the leading (flatter) edge of the base compared to a straight cusp. The curvature and cross-
486 sectional shapes of the cusp shafts may therefore covary to minimise bending stresses experienced during
487 feeding. In all species, the leading edge of the cross-section is wider than the trailing edge, which may act
488 to compensate for the effects of shaft curvature.

489

490 The medial ridge at the base of the central cusp is another interesting source of variation in the species
491 studied. Manual manipulation of 3D prints of the teeth suggests that even the most prominent medial
492 ridge is unlikely to come in to contact with the tongue of the trailing tooth to prevent over-rotation.
493 Instead, we suggest that the presence of the ridge acts to increase the antero-posterior height of the cusp at
494 the base of the shaft, increasing the second moment of area (and thus the resistance to bending) in this
495 direction. We also note from published SEM studies that the relative size and shape of this ridge changes

496 throughout ontogeny, with younger snails tending to have a sharper and more prominent ridge (Herbert et
497 al., 2007, 2015; Pio et al., 2014). Juvenile snails also tend to drill more than their adult counterparts
498 (Herbert et al., 2007; 2016), and therefore might be expected to have tooth shapes that reflect this mode of
499 feeding, or that their teeth need to be more efficient to compensate for their comparatively small size. If
500 the medial ridge is an adaptation for resistance to bending, then this ontogenetic difference is interesting,
501 as paedomorphosis has been observed in muricid radulae before, and implies that heterochronic shifts
502 could be the mechanism by which drilling evolved in this group (Herbert et al., 2007, 2015).

503

504 **4.4.2 Changes in cusp shape and length with wear.** Tooth wear during drilling alters cross-sectional
505 shapes, lengths, and curvature of the central and lateral cusps (Fig. 2), although the effect of wear on
506 drilling performance is unknown. Hickman (1980) points out that the unworn state of a tooth may not
507 represent its most efficient functional shape. The most efficient shape for drilling may instead only arise
508 after some wear has taken place. Recognition of this context may offer further insight on the curvature of
509 radular cusp shafts. During feeding, the radula can be thought of as a cutting tool with rake and clearance
510 angles (Van der Wal et al., 2000). An efficient tool requires these angles to be positive, and, in particular,
511 that the clearance angle stay above zero to allow the tool purchase on the worked surface. Assuming that
512 the animal maintains a consistent feeding stroke, the curvature of the shaft allows a positive clearance
513 angle to remain as the cusp wears. Wear patterns in *T. geversianus* (Fig. 2) suggest that cusps may have
514 distinct mechanical properties between the leading and trailing edges that would cause them to be self-
515 sharpening, although this has not yet been studied. Extreme cusp wear eventually eliminates the cusps
516 altogether but brings the smaller denticles between the cusps and denticles into contact with the prey
517 shell, potentially extending the life of the tooth as a drilling tool (Fig. 2).

518

519 **4.5 Material properties of muricid radulae**

520 Muricid snails build their radulae from chitin, with various degrees of tanning or mineralisation by
521 calcium, silica, strontium, and other trace metals (Carriker and Van Zandt, 1972; Hickman, 1980; Tyler
522 and Schiffbauer, 2012). Tomographic data from the four specimens studied here suggest that the muricid
523 rachidian tooth is homogeneous in composition, with no distinct layers of different elemental composition
524 (e.g., metal), as previously observed in studies of chitons (Wealthall et al., 2005; Weaver et al., 2010). We
525 infer that the muricid rachidian is mostly organic with low mineralisation due to its similarity under X-
526 rays to both the radular ribbon and the PVA mounting glue (SI 1). A caveat in this finding is that
527 synchrotron images cannot easily detect ultrastructural heterogeneities when there is no change in
528 material (Wealthall et al., 2005) or when they are below the 360 nm resolution of the synchrotron (e.g.
529 Weaver et al., 2010; Lu and Barber, 2012; Tyler and Schiffbauer, 2012; Wang et al., 2014).

530

531 **5 CONCLUSIONS**

532 Padilla (2003) outlines three main areas in which to focus future studies of radular form and function,
533 specifically: the quantification of morphology, explicit tests of function, and efforts towards a synthesis of
534 the two. While the small size of the radula has historically presented several challenges in the imaging
535 and functional study of this organ, many of these challenges can now be overcome in light of
536 technological advances in imaging and the field of functional morphology. In any study of functional
537 morphology, a reasonable geometric model of the morphology concerned must first be obtained.
538 Although SEMs offer excellent spatial resolution, they are still two-dimensional images. Synchrotron
539 imaging allows us to capture detailed three-dimensional representations of radular morphology (see also
540 Kruta et al., 2015 for an ammonoid example), offering the chance to observe several new features. Once
541 obtained, these models may then be used in advanced downstream analyses that address each of Padilla's
542 (2003) focal concerns.

543

544 The field of geometric morphometrics has advanced significantly since 2003 (Adams et al., 2013),
545 allowing for the detailed quantification and analysis of organismal form in three dimensions. A potential
546 limitation of landmark-based geometric morphometrics when applied to the radula is a lack of
547 homologous landmark points across taxa, however, advances in the use of 'homology-free' landmarks
548 (e.g., Boyer et al., 2015) mean that geometric morphometrics is a viable tool for the study of this system.
549 In addition to capturing detailed 3D data, synchrotron scanning also has a dramatically higher rate of
550 throughput than other tomographic methods, meaning that the large sample sizes necessary for geometric
551 morphometrics studies may be obtained. The main rate-limiting steps are gaining access to a synchrotron
552 facility and the time taken to segment the tomographic data.

553

554 *In vivo* and *ex vivo* experiments on radula function are difficult to conduct, owing to the radula's small
555 size (although see Padilla, 1985; 1989; Carriker et al., 1974; Krings et al., 2019). Our synchrotron
556 approach can overcome these limitations in two creative ways. The first is that, once segmented, radular
557 teeth are represented as computer surface files suitable for up-scaled 3D printing. This allows for physical
558 models to be produced for *in vitro* experimental work (e.g. Krings et al., 2021d). The second, and more
559 versatile, implication of this is the potential for *in silico* functional testing using finite element analysis
560 (FEA; reviewed in Bright, 2014) and multibody dynamics analysis (MDA; reviewed in Curtis, 2008). The
561 use of deductive and inductive FEA within and between taxa allows specific hypotheses about the stress
562 performance of traits to be tested (Rayfield, 2007). MDA can test hypotheses on likely ranges of motion,
563 and thanks to its collision-detection capabilities, investigate tooth-tooth interactions and the potential for

564 disarticulation. Critically, FEA and MDA can be combined with one another (e.g. Lautenschlager et al.,
565 2018) or with geometric morphometrics (Polly et al., 2016) to build a comprehensive analytical
566 framework in which to interrogate the links between function and form in an evolutionary context. This
567 combination of methodologies therefore allows us to untangle a key problem identified in studies of snail
568 radulae by Hickman (1980): that not all features are necessarily adaptive (indeed, such thinking is
569 problematic across all taxa; see Lauder, 1995).

570

571 **ACKNOWLEDGMENTS**

572 The authors thank the University of South Florida for travel grants to GSH to conduct field work in
573 Panama and Argentina; Jerry Harasewych and Gregorio Bigatti for logistical support of lab and field
574 work in Panama and Argentina, respectively; Vincent Fernandez, Pamela Gill and Julia Schultz for
575 assistance with synchrotron scanning; Fabián Tricarico for assistance with Scanning Electron
576 Microscopy; Philip Morris for help with Avizo; and two reviewers for helpful comments.

577

578 **Conflict of Interest.** The authors declare no conflicts of interest.

579

580 **Author contributions.** concept (Jen Bright, Gregory Herbert, Ryan Carney), specimen collection and
581 preparation (Gregory Herbert, Maria Jose Pio), SEM data collection (Gregory Herbert, Maria Jose Pio),
582 synchrotron data collection (Elis Newham, Jen Bright), 3D reconstructions (Stephen Hill, Amber Carlson,
583 Jen Bright, Ryan Carney); visualisations (Stephen Hill, Amber Carlson, Ryan Carney); interpretation
584 (Stephen Hill, Jen Bright, Gregory Herbert, Ryan Carney); drafting and editing (all authors).

585

586

LITERATURE CITED

587 Adams, D.C., Rohlf, F.J., Slice, D.E. (2013). A field comes of age: geometric morphometrics in the 21st
588 century. *Hystrix, the Italian Journal of Mammalogy*, 24, 7-14.

589

590 Barber, A.H., Lu, D., Pugno, N.M. (2015). Extreme strength observed in limpet teeth. *Journal of the*
591 *Royal Society Interface*, 12, 20141326.

592

593 Boyer, D.M., Puente, J., Gladman, J.T., Glynn, C., Mukherjee, S., Yapuncich, G.S., and Daubechies, I.
594 (2015) A new fully automated approach for aligning and comparing shapes. *The Anatomical Record*. 298,
595 249–276

596

597 Bright, J.A. (2014) A review of paleontological finite element models and their validity. *Journal of*
598 *Paleontology*. 88, 760-769.

599

600 Carney R.M. (in revision) Topological coordinate systems: a joint surface approach for comparative
601 skeletal analysis and scientific motion transfer.

602

603 Carriker, M.R. (1969). Excavation of boreholes by the gastropod, *Urosalpinx*: An analysis by light and
604 scanning electron microscopy. *American Zoologist*, 9, 917-933.

605

606 Carriker, M.R. (1981). Shell penetration and feeding by naticacean and muricacean predatory gastropods:
607 a synthesis. *Malacologia*, 20, 403-422.

608

609 Carriker, M.R., Gruber, G.L. (1999) Uniqueness of the gastropod accessory boring organ (ABO):
610 comparative biology, an update. *Journal of Shellfish Research*, 18, 579-595.

611

612 Carriker, M.R., Schaadt, J.G. (1973). Predatory behavior of the shell-boring snail *Urosalpinx cinerea*: a
613 sound, color, motion picture. MBL Woods Hole. Available from Smithsonian Institution Archives,
614 Accession 08-005, Melbourne R. Carriker Papers.

615

616 Carriker, M.R., Van Zandt, 1972. Predatory behavior of a shell-boring muricid gastropod. in Winn H.E.
617 and Olla, B.L., [Eds.], *Behavior of Marine Animals: Current Perspectives in Research, Vol. 1,*
618 *Invertebrates*. pp.157-244, Plenum Press, New York.

619

620 Carriker, M.R., Schaadt, J.G., Peters, V. (1974) Analysis by slow-motion picture photography and
621 scanning electron microscopy of radular function in *Urosalpinx cinerea follyensis* (Muricidae,
622 Gastropoda) during shell penetration. *Marine Biology*, 25, 63-76.

623

624 Cignoni, P., Callieri, M., Corsini, M., Dellepiane, M., Ganovelli, F., Ranzuglia, G. (2008) MeshLab: an
625 open-source mesh processing tool. *Sixth Eurographics Italian Chapter Conference*, 129-136.

626

627 Cunningham, J.A., Rahman, I.A., Lautenschlager, S., Rayfield, E.J., Donoghue, P.C.J. (2014). A virtual
628 world of paleontology. *Trends in Ecology and Evolution*, 29, 347-357.

629

630 Curtis, N. (2011) Craniofacial biomechanics: an overview of recent multibody modelling studies. *Journal*
631 *of Anatomy*. 218, 16-25.
632

633 Dietl, G.P., Herbert, G.S. (2005). Influence of alternative shell-drilling behaviours on attack duration of
634 the predatory snail, *Chicoreus dilectus*. *Journal of Zoology*, 265, 201-206.
635

636 Donoghue, P.C.J., Bengston, S., Dong, X.-P., Gostling, N.J., Huldtgren, T., Cunningham, J.A., Yin, C.,
637 Yue, z., Peng, F., Stampanoni, M. (2006). Synchrotron x-ray tomographic microscopy of fossil embryos.
638 *Nature*, 44, 680-683.
639

640 Fedosov, A.E., Kantor, Y.I. (2012) A new species and genus of enigmatic turriiform Fascioliariidae from
641 the Central Indo-Pacific (Gastropoda: Neogastropoda). *Archiv für Molluskenkunde International Journal*
642 *of Malacology*, 141, 137-144.
643

644 Fedosov, A.E. Puillandre, N., Kantor, Y.I., Bouchet, P. (2015). Phylogeny and systematics of mitriform
645 gastropods (Mollusca: Gastropoda: Neogastropoda) *Zoological Journal of the Linnean Society*, 175, 336-
646 359.
647

648 Fedosov, A.E., Puillandre, N., Herrmann, M., Dgebuadze, P., Bouchet, P. (2017). Phylogeny, systematics,
649 and evolution of the family Costellariidae (Gastropoda: Neogastropoda). *Zoological Journal of the*
650 *Linnean Society*, 179, 541-626.
651

652 Fedosov, A.E., Caballer Gutierrez, M., Buge, B., Sorokin, P.V., Puillandre., N., Bouchet, P. (2019).
653 Mapping the missing branch on the neogastropod tree of life: molecular phylogeny of marginelliform
654 gastropods. *Journal of Molluscan Studies*, 85, 440-452.
655

656 Fujioka, Y. (1985). Seasonal aberrant radular formation in *Thais bronni* (Dunker) and *T. clavigera*
657 (Küster) (Gastropoda: Muricidae). *Journal of Experimental Marine Biology and Ecology*, 90, 43-54.
658

659 Grunenfelder, L.K., Escobar de Obaldia, E., Wang, Q., Li, D., Weden, B., Salinas, C., Wuhrer, R.,
660 Zavattieri, P., Kisailus, D. (2014). Stress and damage mitigation from oriented nanostructures within the
661 radular teeth of *Cryptochiton stelleri*. *Advanced Functional Materials*, 24, 6093-6104.
662

663 Harasewych, M.G. (1987). A revision of the genus *Benthovoluta* with notes on the evolution of the
664 subfamily Ptychactractinae (Prosobranchia: Turbinellidae). *The Nautilus*, 101, 166-181.
665

666 Harasewych, M.G. (2018). The anatomy of *Tudicla spirillus* (Linnaeus, 1767) and the relationships of the
667 Tudicidae (Gastropoda: Neogastropoda). *The Nautilus*, 132, 35-44.

668 Harding, J.M., Gera, S.M. and Mann, R., 2008. Radula morphology in veined rapa whelks, *Rapana*
669 *venosa* (Valenciennes, 1846 (Gastropoda: Muricidae) from Chesapeake Bay, USA. *Nautilus*, 122, 217-
670 227.

671 Hemingway, G. T. 1975. Functional morphology of feeding in the predatory whelk, *Acanthina spirata*,
672 Gastropoda: Prosobranchia). *Bulletin of the American Malacological Union, Inc.* pp. 64–65 (Abstract).

673 Herbert, G. S. (2004). Observations on diet and mode of predation in *Stramonita biserialis* (Gastropoda:
674 Muricidae) from the northern Gulf of California. *Festivus*, 36, 41-45.
675

676 Herbert, G. S., Dietl, G. P., Fortunato, H., Simone, L. R., & Sliko, J. L. (2009). Extremely slow feeding in
677 a tropical drilling ectoparasite, *Vitularia salebrosa* (King and Broderip, 1832)(Gastropoda: Muricidae), on
678 molluscan hosts from Pacific Panama. *The Nautilus*, 123(3), 121-136.
679

680 Herbert, G.S., Merle, D., Gallardo, C.S. (2007). A developmental perspective on evolutionary innovation
681 in the radula of the predatory Neogastropod family Muricidae. *American Malacological Bulletin*, 23, 17-
682 32.
683

684 Herbert, G.S., Pio, M.J., Pastorino, G., Harasewych, M.G., Kantor, Y., Lamy, D., Pointier, J.-P. (2015).
685 Morphological development of the radula of four species of the Neogastropod family Muricidae.
686 *Malacologia*, 58, 323-336.
687

688 Herbert, G. S., Whitenack, L. B., & McKnight, J. Y. (2016). Behavioural versatility of the giant murex
689 *Muricanthus fulvescens* (Sowerby, 1834)(Gastropoda: Muricidae) in interactions with difficult
690 prey. *Journal of Molluscan Studies*, 82(3), 357-365.
691

692 Hickman, C.S. (1980). Gastropod radulae and the assessment of form in evolutionary paleontology.
693 *Paleobiology*, 6, 276-294.
694

695 Huxley, T.H. (1853). II. On the morphology of the cephalous mollusca, as illustrated by the anatomy of
696 certain heteropoda and pteropoda collected during the voyage of HMS" Rattlesnake" in 1846-50.
697 *Philosophical Transactions of the Royal Society of London*, (143), 29-65.
698

699 Kantor, Y.I., Bouchet, P. (1997). The anatomy and systematics of *Ceratoxancus*, a genus of deep-water
700 Ptychatractinae (Gastropoda: Turbinellidae) with labral spine. *The Veliger*, 40, 101-120.
701

702 Kantor, Y.I., Bouchet, P. (2007). Out of Australia: *Belloлива* (Neogastropoda: Olividae) in the Coral Sea
703 and New Caledonia. *American Malacological Bulletin*, 22, 27-73.
704

705 Kantor, Y.I., Bouchet, P., Oleinik, A. (2001). A revision of the Recent species of *Exilia*, formerly
706 *Benthovoluta* (Gastropoda: Turbinellidae). *Ruthenica*, 11, 81-136.
707

708 Kantor, Y.I., Lozouet, P., Puillandre, N., Bouchet, P. (2014). Lost and found: the Eocene family
709 Pyramimitridae (Neogastropoda) discovered in the recent fauna of the Indo-Pacific. *Zootaxa*, 3754, 239-
710 276.
711

712 Kantor, Y.I., Fedosov, A.E., Puillandre, N., Bonillo, C., Bouchet, P. (2017) Returning to the roots:
713 morphology, molecular phylogeny and classification of the Olivoidea (Gastropoda: Neogastropoda).
714 *Zoological Journal of the Linnean Society*, 180, 493-541.
715

716 Kool, S.P. (1993). Phylogenetic analysis of the Rapaninae (Neogastropoda; Muricidae). *Malacologia*, 35,
717 155-259.
718

719 Krings, W., Faust, T., Kovalev, A., Neiber, M.T., Glaubrecht, M., Gorb, S. (2019). In slow motion: radula
720 motion pattern and forces exerted to the substrate in the land snail *Cornu aspersum* (Mollusca,
721 Gastropoda) during feeding. *Royal Society Open Science*, 6, 190222.
722 <http://dx.doi.org/10.1098/rsos.190222>
723

724 Krings, W., Marcé-Nogué, J., Karabacak, H., Glaubrecht, M., Gorb, S.N. (2020). Finite element analysis
725 of individual taenioglossan radular teeth. *Acta Biomaterialia*, 115, 317-332.
726

727 Krings, W., Kovalev, A., Gorb, S.N. (2021a). Influence of water content on mechanical behaviour of
728 gastropod taenioglossan radulae. *Proceedings of the Royal Society B*, 288, 20203171.

729
730 Krings, W., Kovalev, A., Gorb, S.N. (2021b). Collective effect of damage prevention in the taenioglossan
731 radular teeth is related to the ecological niche in Paludomidae (Gastropoda: Cerithioidea). *Acta*
732 *Biomaterialia*, 135, 458-472.

733
734 Krings, W., Marcé-Nogué, J., Gorb, S.N. (2021c). Finite element analysis relating shape, material
735 properties, and dimensions of taenioglossan radular teeth with trophic specialisations in Paludomidae
736 (Gastropoda). *Scientific Reports*, 11, 22775.

737
738 Krings, W., Karabacak, H., Gorb, S.N. (2021d). From the knitting shop: the first physical and dynamic
739 model of the taenioglossan radula (Mollusca: Gastropoda) aids in unravelling functional principles of the
740 radular morphology. *Journal of the Royal Society Interface*, 18, 20210377.
741 <https://doi.org/10.1098/rsif.2021.0377>

742
743 Krings, W., Matsumura, Y., Brütt, J.-O., Gorb, S.N. (2022a). Material gradients in gastropod radulae and
744 their biomechanical significance: a combined approach on the paludomid *Lavigeria grandis*. *The Science*
745 *of Nature*, 109, 52. <https://doi.org/10.1007/s00114-022-01822-9>

746
747 Krings, W., Brütt, J.-O., Gorb, S.N. (2022b). Ontogeny of the elemental composition and the
748 biomechanics of radular teeth in the chiton *Lepidochitona cinerea*. *Frontiers in Zoology*, 19, 19.
749 <https://doi.org/10.1186/s12983-022-00465-w>

750
751 Kruta, I., Landman, N.H., Tanabe, K. (2015). Ammonoid radula. In Klug, C., Korn, D., De Baets, K.,
752 Kruta, I., Mapes, R. [eds] *Ammonoid Paleobiology: From anatomy to ecology*. Topics in Geobiology, vol
753 43. Springer, Dordrecht. https://doi.org/10.1007/978-94-017-9630-9_11

754
755 Lauder, G.V. (1995). On the inference of function from structure. in Thomason, J.J. [ed] *Functional*
756 *Morphology in Vertebrate Paleontology*. pp. 1-18. Cambridge University Press, Cambridge, UK.

757
758 Lautenschlager, S. (2016). Reconstructing the past: methods and techniques for the digital restoration of
759 fossils. *Royal Society Open Science*, 3, 160342. <https://doi.org/10.1098/rsos.160342>

760
761 Lautenschlager, S., Gill, P.G., Luo, Z.-X., Fagan, M.J., and Rayfield, E.J. (2018) The role of
762 miniaturization in the evolution of the mammalian jaw and middle ear. *Nature*. 561, 533-537.

763
764 Lee, J.-E., Connolly, J., Yang, W., Freychet, G., Wang, T., Herrera, S.A., Murata, S., Dasika, P.S.,
765 Montroni, D., Pohl, A., Zhu, C., Zhernenkov, M., Wuhrer, R., Sheppard, L., Nemoto, M., Arakaki, A.,
766 Zavattieri, P., Kisailus, D. (2023) Fibrous anisotropy and mineral gradients within the radula stylus of
767 chiton: controlled stiffness and damage tolerance in a flexible biological composite. *Journal of Composite*
768 *Materials*, 57, 565-574.
769
770 Lu, D., & Barber, A.H. (2012). Optimized nanoscale composite behaviour in limpet teeth. *Journal of the*
771 *Royal Society Interface*, 9, 1318-1324.
772
773 Marcé-Nogué, J. (2022). One step further in biomechanical models in palaeontology: a nonlinear finite
774 element analysis review. *PeerJ*, 10, e13890. <https://doi.org/10.7717/peerj.13890>
775
776 Padilla, D.K. (1985). Structural resistance of algae to herbivores. *Marine Biology*. 90, 103-109.
777
778 Padilla, D.K. (1989). Algal structure defenses: form and calcification in resistance to tropical limpets.
779 *Ecology*. 70, 835-842.
780
781 Padilla, D.K. (1998). Inducible phenotypic plasticity of the radula in *Lacuna* (Gastropoda: Littorinidae).
782 *The Veliger*, 41, 201-204.
783
784 Padilla, D.K. (2001). Food and environmental cues trigger an inducible offence. *Evolutionary Ecology*
785 *Research*, 3, 15-25.
786
787 Padilla, D.K. (2003). Form and function of radular teeth of herbivorous molluscs: focus on the future.
788 *American Malacological Bulletin*. 18, 163-168.
789
790 Paul, S., Herbert, G. S., & Dietl, G. P. (2015). Predator-induced edge-drilling behaviour of *Chicoreus*
791 *dilectus* (Gastropoda: Muricidae). *Journal of Molluscan Studies*, 81(2), 233-237.
792
793 Pio, M.J., Herbert, G.S., & Pastorino, G. (2014). Developmental origins of complex radular characters in
794 the Muricidae: the bifid rachidian edge. *Invertebrate biology*, 133(1), 64-73.
795

796 Pio, M.J., Mendez, M.M., Galván, D.E., Bigatti, G., West, K., Herbert, G.S. (2019). Does the native
797 predator *Trophon geversianus* exert top-down control on the invasive barnacle *Balanus glandula* on
798 Patagonian rocky shores? *Marine and Freshwater Research*, 70, 1552-1560.
799

800 Polly, P.D., Stayton, C.T., Dumont, E.R., Pierce, S.E., Rayfield, E.J., Angielczyk, K.D. (2016).
801 Combining geometric morphometrics and finite element analysis with evolutionary modeling: towards a
802 synthesis. *Journal of Vertebrate Paleontology*, 36, e1111225.
803

804 Ponder, W.F., & Taylor, J.D. (1992). Predatory shell drilling by two species of *Austroginella*
805 (Gastropoda: Marginellidae). *Journal of Zoology*, 228(2), 317-328.
806

807 Puillandre, N., Fedosov, A. E., & Kantor, Y. I. (2017). Systematics and Evolution of the Conoidea 17.
808 Evolution of venomous animals and their toxins, 367.
809

810 Rayfield, E.J. (2007). Finite element analysis and understanding the biomechanics and evolution of living
811 and fossil organisms. *Annual Review of Earth and Planetary Sciences*, 35, 541-576.
812

813 Solem, A., (1972). Malacological applications of scanning electron microscopy II. Radular structure and
814 functioning. *The Veliger*, 14, 327-336.
815

816 Solem, A., (1973). Convergence in pulmonate radulae. *The Veliger*, 15, 165-171.
817

818 Taylor, J.D. (1998). Understanding biodiversity: adaptive radiations of predatory marine gastropods. *in*
819 Morton, B. [Ed.] *The Marine Biology of the South China Sea*. Proceedings of the Third International
820 Conference on the Marine Biology of the South China Sea, pp. 187-206. Hong Kong University Press,
821 Hong Kong.
822

823 Tyler, C.L., Schiffbauer, J.D. (2012). The fidelity of microstructural drilling predation traces to gastropod
824 radula morphology: paleoecological applications. *Palaios*, 27, 658-666.
825

826 Van der Wal, P., Geisen, H.J., Videler, J.J. (2000). Radular teeth as models for the improvement of
827 industrial cutting devices. *Materials Science and Engineering C*, 7, 129-142.
828

829 Vermeij, G.J. (1977) The Mesozoic marine revolution: evidence from snails, predators and grazers.
830 *Paleobiology*, 3, 245-258.
831
832 Vermeij, G.J. (2001). Innovation and evolution at the edge: origins and fates of gastropods with a labral
833 tooth. *Biological Journal of the Linnean Society*, 72, 461-508.
834
835 Vermeij, G.J., Carlson, S.J. (2000). The muricid gastropod subfamily Rapaninae: phylogeny and
836 ecological history. *Paleobiology*, 26,19-46.
837
838 Wang, C., Li, Q.Y., Wang, S.N., Qu, S.X., Wang, X.X. (2014). Microstructure and self-sharpening of the
839 magnetite cap in chiton tooth. *Materials Science and Engineering C*, 37, 1-8.
840
841 Wealthall, R.J., Brooker, L.R., Macey, D.J., Griffin, B.J. (2005). Fine structure of the mineralized teeth of
842 the chiton *Acanthopleura echinata* (Mollusca: Polyplacophora). *Journal of Morphology*, 265, 165-175.
843
844 Weaver, J.C., Wang, Q., Miserez, A., Tantuccio, A., Stromberg, R., Bozhilov, K.N., Maxwell, P., Nay,
845 R., Heier, S.T., DiMasi, E., Kisailus, D. (2010). Analysis of an ultra hard magnetic biomineral in chiton
846 radular teeth. *Materials Today*, 13, 42-52.
847